

# Modelling Radiation Effects Using the Ab-initio Based Tungs Potentials

C. Björkas<sup>a,\*</sup>, K. Nordlund<sup>a</sup>, and S. Dudarev<sup>b</sup>

<sup>a</sup>Association EURATOM-Tekes, Department of Physics,  
P.O. Box 43, FI-00014 University of Helsinki, Finland and

<sup>b</sup>Theory and Modelling Department, EURATOM/UKAEA Fusion Association,  
Culham Science Centre, Oxfordshire OX14 3DB, UK

The Embedded Atom Model (EAM) Derlet-Nguyen-Manh-Dudarev tungsten and vanadium potentials were modified to correctly reproduce the experimentally obtained defect threshold energies. This was done by letting the interactions at short distances be dictated by the universal screened Coulomb potential. Both the repulsive part and the electron density function of the potentials were modified. The potentials were then used in collision cascade simulations and the resulting defects were compared with the corresponding defects in iron. Based on this comparison, factors affecting the outcome of a cascade were identified.

PACS numbers: 61.72.Ji, 28.52.Fa, 61.80.Hg, 34.20.Cf

Keywords: Vanadium, Tungsten, Iron, Interatomic potentials, Molecular dynamics simulations, Fusion reactor materials

## I. INTRODUCTION

Structural materials in a fusion power plant will be subjected to neutron irradiation, which affects the lifetime of components because of radiation damage that neutrons generate in the materials. Understanding, assessing and, desirably, predicting the type of the damage is one of the significant directions of fusion materials research, and Molecular Dynamic (MD) simulations is one of the effective and powerful tools capable of addressing the problem. Simulations of irradiation phenomena in tungsten and vanadium is of particular interest. This is because, owing to its low tritium retention and low sputtering yield [1], tungsten has been chosen as divertor material in the fusion reactor ITER [2], and vanadium alloys are among promising candidate materials for the first-wall and blanket applications, due to their excellent thermal and activation properties [3].

Interatomic potentials provide crucially important input to MD simulations, and correct description of not only equilibrium but also of defect properties are required before a potential can be used to model more complex collective events and processes. The short-range part of a potential is of particular significance when dealing with high-energy interactions. In this work we have modified the repulsive part of two recently parametrized potentials for vanadium and tungsten [4]. The potentials reproduce the correct point defect structures and, after suitable modification, they also describe well the observed experimental threshold energies.

We also performed simulations of recoil cascades in V and W. The resulting primary damage was compared to that in Fe where a similar potential and same simulation and analyzing methods were used [5, 6]. This gives insight into the effect of the geometric structure of radiation defects, since V and Fe are similar in atomic

mass and threshold energies, but differ when it comes to the structure of the most stable interstitial configuration. In vanadium the  $\langle 111 \rangle$  crowdion is the ground structure [4, 7], while the  $\langle 110 \rangle$  dumbbell is the most stable in body-centred cubic iron [5, 6, 8]. The ground state interstitial in tungsten is also the  $\langle 111 \rangle$  crowdion, and in addition tungsten differs strongly from vanadium and iron in terms of the atomic mass, threshold energies and defect formation energies.

In addition to the identification of similarities and differences between radiation damage created in the three bcc metals noted above, we note a significant pragmatic aspect of systematic MD investigation of radiation damage in these three materials. Predicting microstructural changes in materials under neutron irradiation requires relating the incident flux of neutrons bombarding the material with the concentration of radiation defects produced by neutron impacts. In engineering applications semi-empirical rules are often used, for example, the Norgett-Robinson-Torrens (NRT) model [9] where the number of defects generated by fast neutrons is assumed to be proportional to the energy of neutrons initiating collision cascades, and inversely proportional to the threshold Frenkel pair formation energy. Finding the pre-factor in the NRT equation determining the rates of formation of Frenkel pairs in materials under irradiation requires carrying out atomistic simulations similar to those described below.

## II. METHOD

### A. Modification of the repulsive part

A merging interpolation function  $V_{int}(r)$  was used to spline the universal potential of Ziegler, Biersack and Littmark  $V_{ZBL}(r)$  [10] with the original tungsten and vanadium pair potentials  $V_{orig}^{W,V}(r)$ . This approach was also used for iron in Ref. [6]. The modified repulsive potentials thus take the form

---

\*Electronic address: carolina.bjorkas@acclab.helsinki.fi

$$\begin{aligned}
V_{BN}^{W,V}(r) &= V_{ZBL}^{W,V}(r), \quad r \leq r_1^{W,V} \\
&= V_{int}^{W,V}(r), \quad r_1^{W,V} < r < r_2^{W,V} \\
&= V_{orig}^{W,V}(r), \quad r \geq r_2^{W,V}
\end{aligned} \quad (1)$$

where  $r_1$  and  $r_2$  are the cutoffs for the interpolation functions. These cutoffs were fitted in order to get the threshold energies correct without affecting the interstitial energies. The interpolation function is a fifth order polynomial,

$$V_{int}(r) = a_0 + a_1 r + a_2 r^2 + a_3 r^3 + a_4 r^4 + a_5 r^5 \quad (2)$$

which was constructed to give a continuous potential and first and second derivatives at  $r_1$  and  $r_2$ .

## B. Modification of the electron density function

The electron density function  $f(r)$  in both potentials was also modified. This was done to better correctly reproduce the contribution of the attractive electron d-states. The electron density in the EAM formalism is of the expression

$$\rho_i = \sum_{j,j \neq i} f(r_{ij}), \quad (3)$$

and it contributes to the embedding energy through  $F(\rho) = -A\sqrt{\rho}$ , where  $A$  is a fitted constant found in Ref. [4]. The modified density function  $f_{BN}^{W,V}(r)$  looks like

$$\begin{aligned}
f_{BN}^{W,V}(r) &= \rho_0^{W,V}, \quad r \leq r_3^{W,V} \\
&= \rho_{int}^{W,V}(r), \quad r_3^{W,V} < r < r_4^{W,V} \\
&= \rho_{orig}^{W,V}(r), \quad r \geq r_4^{W,V}.
\end{aligned} \quad (4)$$

$\rho_{orig}$  is equation 2 Ref. [4] and the  $\rho_{int}$  is a third order polynomial

$$\rho_{int}(r) = b_0 + b_1 r + b_2 r^2 + b_3 r^3, \quad (5)$$

which was constructed assuming that the bonding part of the potential approaches a constant value for interatomic distances smaller than  $r_3$ , and that it smoothly joins the original density function at  $r_4$ . The cutoff radii  $r_3$  and  $r_4$  for the interpolation procedure were determined by requirement that the bonding part of the potential does not diverge in the limit of small separation between atoms, and instead it saturates in this limit. The characteristic interatomic distance at which this saturation occurs is related to the spatial extent of overlapping d-orbitals (the 3d orbitals in the case of vanadium atoms and 5d orbitals in the case of tungsten atoms), which provide the dominant contribution to the cohesive energy in these transition metals. Figs. 2 and 3 show normalized radial distributions of electron density in the atomic orbitals of vanadium or tungsten atoms, calculated by solving the relativistic Dirac equation in the local spin density approximation. These distributions were used for assessing the values of the cutoff radii  $r_3$  and  $r_4$ .

## C. Molecular dynamics simulations

The threshold energies were calculated as in Ref. [11] and the collision cascades in V and W were initiated by recoils with energies in the range 0.5 – 20 keV. The methods are the same as in Ref. [6] to enable direct comparison with Fe.

The cascade damage was analyzed in terms of total amount of Frenkel pairs and defect in clusters. Vacancies closer than second nearest neighbour (nn) distance and interstitials closer than third nn distance were defined as belonging to the same defect cluster.

The interstitial defect migration energies were determined dynamically by following the mean square displacements  $\langle R^2 \rangle$  over a period of time  $t$ . The diffusivity was calculated according to  $D = \frac{\langle R^2 \rangle}{6t}$  and the migration energies were determined by fitting Arrhenius laws to the diffusivity data. The temperature range was 300 to 550 K.

## III. RESULTS AND DISCUSSION

### A. Potential modifications and threshold energies

The resulting cutoff values used in Eq. 1 for V and W are found in Tab. I. Although  $r_1$  in vanadium is larger than the distance between two atoms in the shortest interstitial configuration, the modification did not affect its formation energy ( $E_{\langle 111 \rangle}^f = 3.32$  eV). The constants used in the interpolation polynomial (Eq. 2) are given in table II. In Fig. 1 the resulting modification of the potentials is illustrated. Following the modifications, the potential for V is “harder” and the W potential is “softer”.

In vanadium, a reduction of the ZBL potential with a constant  $V_0 = 10$  eV was found to be necessary to obtain realistic values for the threshold displacement energies. The electronic structure calculations on which the ZBL potential is based are optimized only for high-energy interactions, and are not meaningful at energies of a few eV. Hence introducing a small shift in the ZBL potential as a fitting parameter can be done without altering the physically meaningful part of the potential. Note, moreover, that the atom dynamics is only governed by the forces  $dV/dr$  between atoms, and hence the introduction of the constant does not change the atom trajectories in high-energy collisions.

The density function cutoffs used in Eq. 4 are found in Tab. I and the polynomial constants (Eq. 5) in Tab. II.

Table III comprises of the threshold simulation results and available experimental data. The threshold energies of the original potentials were too low and too high in vanadium and tungsten, respectively. Now, both the global minimum and the direction specific minima are in close agreement with the experimental values.

## B. Primary damage

Results from the analyze of the collision cascade damage are illustrated in Fig. 4 to Fig. 9. Results from cascades in Fe done earlier [6] are also included for comparison.

Fig. 4 reveals that there are differences between the Frenkel pair production of the potentials. Fe and V produce almost the same amount at each energy, whereas the amount is clearly smaller in W. This can be related to differences in the defect formation energies: in V and Fe the SIA formation energies are in the range 3.3 – 4.2 eV and the vacancy formation energies are 1.97 eV (Fe) and 2.51 eV (V), whereas for W, these values are 9.548 – 11.68 eV (SIA) and 3.56 eV (vacancy) [4]. The higher the values are, the more energy is required to create the same amount of defects. Differences in threshold displacement energies are not believed to have the same importance [12].

The cascade efficiency (inset in Fig. 4) is the ratio between the number of Frenkel pairs produced in the cascades and the NRT prediction,  $N_{FP}^{NRT} = F_{D_n}/2E_d$  [9].  $F_{D_n}$  equals the recoil energy since no electronic stopping was used and  $E_d$  is the average threshold energy ( $E_d(Fe) = 35$  eV [6],  $E_d(V) = 55$  eV and  $E_d(W) = 85.4$  eV). A similar behaviour is seen in for all elements, namely a decrease of the efficiency with increasing energy.

The Frenkel pair production as a function of time during 10 keV cascades is illustrated in Fig. 5. W is seen to have the lowest amount throughout the cascade, which is related to the discussion above. The recombination in both Fe and W is large. V differs slightly, since here the peak is reached faster and the recombination is smaller. Visualization of the cascades revealed that the cascades in V are very spread out and subcascades are formed already at 10 keV. The somewhat larger lattice parameter and slightly smaller mass of V ( $m^V = 50.94u$ ,  $a_0^V = 3.040$  Å) compared to Fe ( $m^{Fe} = 55.85u$ ,  $a_0^{Fe} = 2.866$  Å) explain why the subcascade threshold is lower in V. This also leads to smaller heat spikes in V, explaining both the fast cooling and fast recombination.

Differences between the elements are found when comparing the interstitial cluster fraction as a function of recoil energy (Fig. 6). The fraction is about 30% at all energies in V, which is explained by the subcascade formation already at 10 keV. A break-up of a cascade into smaller ones effectively hinders large clusters to form. As opposed to V, the cluster fraction increases for both Fe and W. W shows the largest increase, starting from about 9% at 0.5 keV and ending up at about 72% at 20 keV. In order to explain this behaviour, the time evolution of the fraction was studied (see Fig. 7). After the collisional phase (after about 1 ps) the fraction is seen to diminish due to recombination in all potentials. However, the decrease of the clusters in W is very small when compared to V and Fe. This can be related to the very fast movement of the ground state SIA in W, since the

mobility activation energy of the  $\langle 111 \rangle$  crowdion in W is only  $0.03 \pm 0.002$  eV. (In Ref. [4] this energy was determined to 0.013 eV by also taking the local drift motion into account.) On the other hand, the ground state SIA in Fe is the  $\langle 110 \rangle$ -dumbbell with a high activation energy of about 0.26 eV. The fast migration makes it possible for the interstitials to find each other and form clusters.

The SIA mobility activation energy in V was determined to be  $0.079 \pm 0.005$  eV. Note that the V and W energies were calculated only up to 550 K, since at high temperatures the migration behaviour is strongly non-Arrhenius and includes 3D motion. This was also observed for V in Ref. [13] and W in Ref. [4].

A study of the clusters of the other defect type, vacancies, also reveals some dissimilarities. Here W, again, shows deviating behaviour, since the fraction of vacancies in clusters is seen to diminish as a function of recoil energy (see Fig. 8). V and Fe behave similarly, with a constant fraction of about 35%. Looking at the behaviour during 10keV cascades (Fig. 9), one can see that the fraction in W decreases much more than in V and Fe during the recombination phase. This is attributed to the higher melting point of W ( $3775 \pm 50$  K) when compared to V ( $2350 \pm 50$  K) and Fe ( $2125 \pm 25$  K). A high melting point makes the recrystallization front, that pushes vacancies towards the center of a cascade, to move faster [14, 15]. This, in turn, leads to that the vacancies freeze in the lattice instead of migration to the center to form clusters. Hence, a high melting point leads to a low vacancy cluster fraction. At low energies no heat spike liquid zone exists and thus no recrystallization front. This explains why the differences between the potentials are only seen at high energies.

## IV. CONCLUSIONS

The recent *ab initio*-based V and W potentials were modified to be suitable for high-energy simulations. Collision cascades were performed and a comparison between the resulting damage in V, W and Fe revealed elemental differences. These differences were attributed to differences in melting points, defect formation energies, migration energies and subcascade thresholds. The cascade efficiency was, however, seen to be the same ( $\sim 20\%$  at high energies) in all three elements.

## V. ACKNOWLEDGMENTS

This work, supported by the European Communities under the contract of Association between EURATOM/Tekes, was carried out within the framework of the European Fusion Development Agreement. The views and opinions expressed herein do not necessarily reflect those of the European Commission.

- 
- [1] V. Barabash, G. Federici, R. Matera, A. R. Raffray, and ITER Home Teams, *Physica Scripta* Volume T 81 (1999) 74.
- [2] ITER Physics Basis Editors, ITER Physics Expert Group Chairs and Co-Chairs and ITER Joint Central Team and Physics Integration Unit, *Nuclear Fusion* 39 (1999) 2137.
- [3] J. Kurtz, K. Abe, V. M. Chernov, V. A. Kazakov, G. E. Lucas, H. Matsui, T. Muroga, G. R. Odette, D. L. Smith, and S. J. Zinkle, *Journal of Nuclear Materials* 283-287 (2000) 70.
- [4] P. M. Derlet, D. Nguyen-Manh, and S. L. Dudarev, *Phys. Rev. B* 76 (2007) 054107.
- [5] S. L. Dudarev and P. M. Derlet, *J. Phys.: Condens. Matter* 17 (2005) 1.
- [6] C. Björkas and K. Nordlund, *Nuclear Instruments and Methods in Physics Research B* 259 (2007) 853.
- [7] D. Nguyen-Manh, A. P. Horsfield, and S. L. Dudarev, *Physical Review B* 73 (2006) 024103.
- [8] C. Domain and C. S. Becquart, *Physical Review B* 65 (2001) 024103.
- [9] M. J. Norgett, M. T. Robinson, and I. M. Torrens, *Nucl. Engr. and Design* 33 (1975) 50.
- [10] J. F. Ziegler, J. P. Biersack, and U. Littmark, *The Stopping and Range of Ions in Matter*, Pergamon, New York, 1985.
- [11] K. Nordlund, J. Wallenius, and L. Malerba, *Nucl. Instr. Meth. Phys. Res. B* 246 (2006) 322.
- [12] L. Malerba.
- [13] L. Zepeda-Ruiz, J. Rottler, S. Han, G. Ackland, R. Car, and D. Srolovitz, *Physical Review B* 70 (2004) 060102.
- [14] K. Nordlund, M. Ghaly, and R. S. Averback, *J. Appl. Phys.* 83 (1998) 1238.
- [15] K. Nordlund and R. S. Averback, *Phys. Rev. B* 59 (1999) 20.
- [16] F. Maury, M. Biget, P. Vajda, A. Lucasson, and P. Lucasson, *Radiation Effects* 38 (1978) 53.
- [17] H. Neely, D. W. Keefer, and A. Sosin, *Physica Status Solidi* 28 (1968) 675.
- [18] J. A. DiCarlo and J. T. Stanley, *Nasa Report TN D-6464* (1971).
- [19] E. A. Kenik and T. E. Mitchell, *Philosophical Magazine* 32 (1975) 815.
- [20] M. G. Miller and R. L. Chaplin, *Radiation Effects and Defects in Solids* 22 (1974) 99.
- [21] P. Jung and G. Lucki, *Radiation Effects and Defects in Solids* 26 (1975) 99.

Table I: Cutoffs in Å for the interpolation polynomials.  $r_1$  and  $r_2$  are used in the repulsive potential interpolation,  $r_3$  and  $r_4$  in the density function interpolation. The  $\rho_0$  used in the electron density function modification and the shortest distance between two atoms in an interstitial configuration are also given.

	$r_1$	$r_2$	$r_3$	$r_4$	$r_{\langle 111 \rangle}$	$\rho_0$
W	1.10002200044	2.2500450009	1.5000300006	1.80003600072	2.28	10.0064910346
V	0.85001700034	2.10004200084	1.05002100042	1.30002600052	2.0	9.92285513058

Table II: Polynomial coefficients of the interpolation functions for tungsten and vanadium, eq. (2) and (5).

n	$a_n^W$	$b_n^W$	$a_n^V$	$b_n^V$
0	$1.384158153390557 \cdot 10^4$	$-0.659035020672109 \cdot 10^3$	$0.481114923981019 \cdot 10^4$	$0.315794835330294 \cdot 10^2$
1	$-3.580948686976579 \cdot 10^4$	$1.199684049310425 \cdot 10^3$	$-1.442929495827347 \cdot 10^4$	$-0.849624405029494 \cdot 10^2$
2	$3.720306176683384 \cdot 10^4$	$-0.707527073754107 \cdot 10^3$	$1.753254942221297 \cdot 10^4$	$1.029027394065896 \cdot 10^2$
3	$-1.923831128499638 \cdot 10^4$	$0.136726326994010 \cdot 10^3$	$-1.058481288061244 \cdot 10^4$	$-0.396469807405803 \cdot 10^2$
4	$0.493430401777675 \cdot 10^4$		$0.315140381503299 \cdot 10^4$	
5	$-0.050165283774299 \cdot 10^4$		$-0.036943173076800 \cdot 10^4$	

Table III: Threshold displacement energies in eV as predicted by the different potentials.  $N_{direction}$  is the number of directions that was used in determining the minimum  $E_d(\theta, \phi)$  and the average threshold  $E_{d,ave}^{av}$ . The uncertainty of the values (except for the average threshold) is due to the energy steps used in the calculations. The direction specific thresholds are calculated in an interval of 0.2 Miller index around the principal directions. The simulated thresholds were obtained at 4 K and 20 K for tungsten and vanadium, respectively. Available experimental values are also included.

	$N_{directions}$	$E_d(\theta, \phi)$			$E_{d,ave}^{av}$		
		All	$\langle 100 \rangle$	$\langle 110 \rangle$		$\langle 111 \rangle$	
W	Unmodif.	680	55±3	55±3	>100	93±3	88.3±0.7
	Modif.	1096	41±1	41±1	93±1	41±1	84.5±0.9
	Exp.		42±1 <sup>a</sup> (< 7 K), 42±1 <sup>b</sup> (4 K), 50±2 <sup>c</sup> (350 K)	40±2 <sup>a</sup>		44±1 <sup>a</sup>	
V	Unmodif.	2713	13±3	13±3	19±3	13±3	19.6±1.8
	Modif.	1561	23±1	23±1	43±1	41±1	55.0±0.6
	Exp.		30 <sup>d</sup> (295 K), 26±2 <sup>e</sup> (4 K), 25±2 <sup>f</sup> (20 K)	30 <sup>d</sup>	39 <sup>d</sup>	34 <sup>d</sup>	

<sup>a</sup>Ref. [16]

<sup>b</sup>Ref. [17]

<sup>c</sup>Ref. [18]

<sup>d</sup>Ref. [19]

<sup>e</sup>Ref. [20]

<sup>f</sup>Ref. [21]

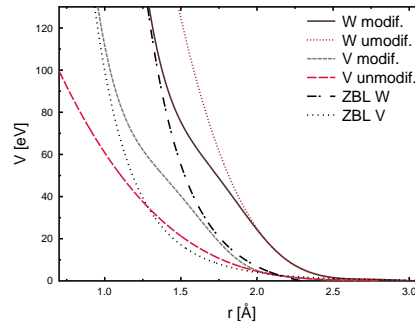


Figure 1: The original and modified repulsive potentials for vanadium and tungsten. The universal ZBL potentials are also included.

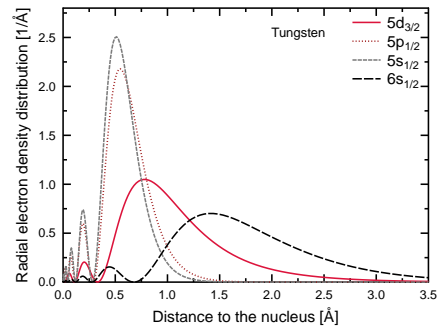


Figure 2: The radial electron density distribution of tungsten.

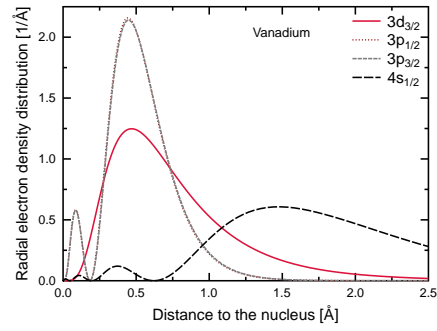


Figure 3: The radial electron density distribution of vanadium.

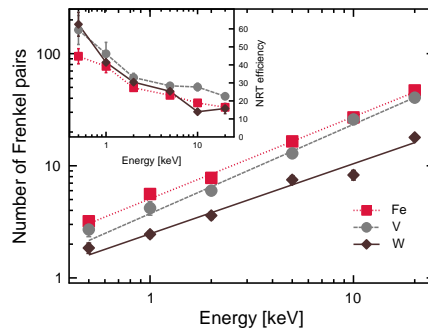


Figure 4: The number of Frenkel pairs after cascades in Fe, V and W, as a function of recoil energy. The inset shows the NRT cascade efficiency (see text)

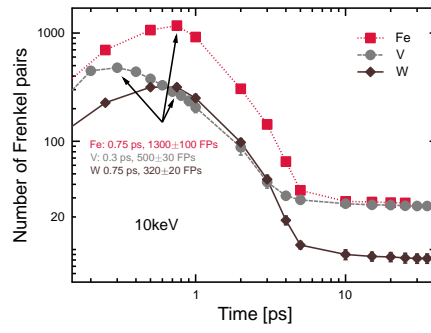


Figure 5: The number of Frenkel pairs as a function of time during 10keV cascades in Fe, V and W.

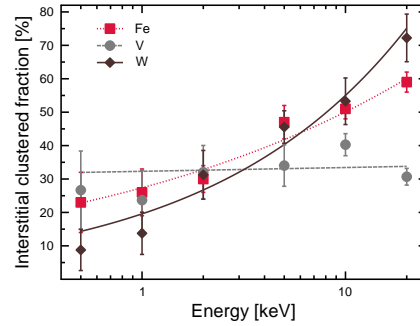


Figure 6: The interstitial clustered fraction in Fe, V and W following collision cascades.

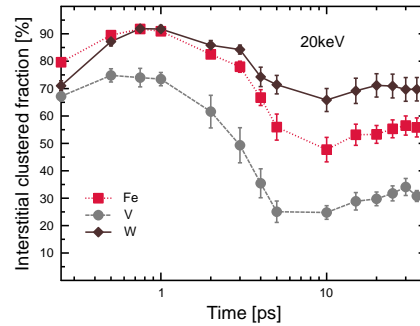


Figure 7: The fraction of interstitials in clusters as a function of time during 20 keV cascades in Fe, V and W.

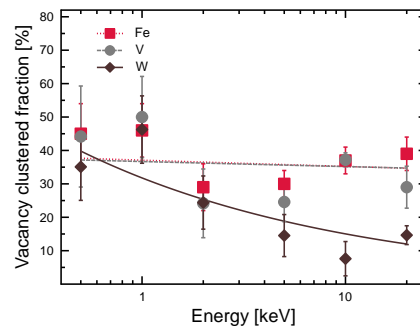


Figure 8: The vacancy clustered fraction in Fe, V and W following collision cascades.

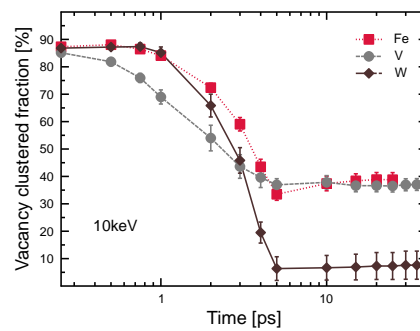


Figure 9: The fraction of vacancies in clusters as a function of time during cascades in Fe, V and W.



Contents lists available at ScienceDirect

## Nuclear Instruments and Methods in Physics Research B

journal homepage: [www.elsevier.com/locate/nimb](http://www.elsevier.com/locate/nimb)

## Erratum

## Erratum to: "Modelling radiation effects using the ab-initio based tungsten and vanadium potentials" [Nucl. Instr. and Meth. B 267 (2009) 3204–3208]

C. Björkas<sup>a,\*</sup>, K. Nordlund<sup>a</sup>, S. Dudarev<sup>b</sup><sup>a</sup>Association EURATOM-Teles, University of Helsinki, Department of Physics, P.O. Box 43, FI-00014, Finland<sup>b</sup>Citlum Centre for Fusion Energy, Abingdon, Oxfordshire OX14 3DB, UK

## 1. Corrections

Due to a mixup, wrong interpolation parameters for W were published in Tables 1 and 2. The correct tables should be as below. For the same reason, the cascade simulations in W were performed with the erroneous potential. However, the difference between the two potential versions is very small (see Fig. 1) and the cascade results were found to be the same within the statistical uncertainties.

In addition to this, the ZBL potential was not reduced by 10 eV for the V potential modification as stated. Instead, it was increased by the same amount.

The threshold calculations were performed with the correct potential and no conclusions are affected by the changes.

We thank M.Sc. H. Wen and Dr. M. Karolewski for bringing the errors to our attention.

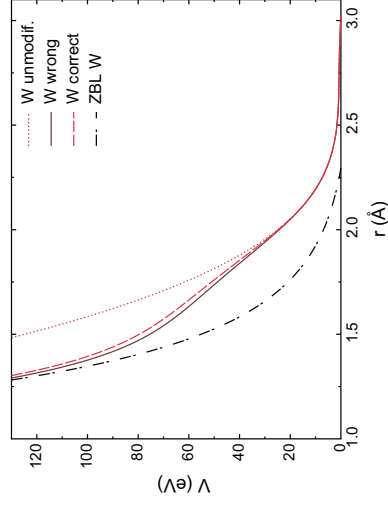


Fig. 1. The universal ZBL potential, the original and modified repulsive potentials for tungsten.

**Table 1**  
Coeffs in Å for the interpolation polynomials.  $r_1$  and  $r_2$  are used in the repulsive potential interpolation.  $r_3$  and  $r_4$  in the density function interpolation. The  $\rho_0$  used in the electron density function modification and the shortest distance between two atoms in an interstitial configuration are also given.

	$r_1$	$r_2$	$r_3$	$r_4$	$r_{\text{int}}$	$\rho_0$
W	1.10002200044	2.10004200084	1.50003000006	1.80003600072	2.28	10.0064910346
V	0.85001700034	2.10004200084	1.05002100042	1.30002600052	2.0	9.92285513058

**Table 2**  
Polynomial coefficients of the interpolation functions for tungsten and vanadium.

$n$	$a_n^W$	$b_n^W$	$a_n^V$	$b_n^V$
0	1.389653276380862 · 10 <sup>4</sup>	-0.659035020672109 · 10 <sup>3</sup>	0.48114923981019 · 10 <sup>4</sup>	0.315794835330294 · 10 <sup>2</sup>
1	-3.596912431628216 · 10 <sup>4</sup>	1.199684049310425 · 10 <sup>3</sup>	-1.442929495827347 · 10 <sup>4</sup>	-0.849524405029494 · 10 <sup>2</sup>
2	3.739206756369099 · 10 <sup>4</sup>	-0.707527073754107 · 10 <sup>3</sup>	1.75325494221297 · 10 <sup>4</sup>	1.029027394065896 · 10 <sup>2</sup>
3	-1.933748081656593 · 10 <sup>4</sup>	0.136726326994010 · 10 <sup>3</sup>	-1.058481288061244 · 10 <sup>4</sup>	-0.396469807405803 · 10 <sup>2</sup>
4	0.495516793802426 · 10 <sup>4</sup>		0.315140381503299 · 10 <sup>4</sup>	
5	-0.050264585985867 · 10 <sup>4</sup>		-0.036943173076800 · 10 <sup>4</sup>	

DOI of original article: 10.1016/j.nimb.2009.06.123

\* Corresponding author.

E-mail address: [carolina.bjorkas@helsinki.fi](mailto:carolina.bjorkas@helsinki.fi) (C. Björkas).0168-583X/\$ - see front matter © 2010 Published by Elsevier B.V.  
doi:10.1016/j.nimb.2010.01.011